

Article

Versatile Synthesis of Pd and Cu Co-Doped Porous Carbon Nitride Nanowires for Catalytic CO Oxidation Reaction

Kamel Eid , Yahia H. Ahmad, Assem T. Mohamed , Anas G. Elsafy 
and Siham Y. Al-Qaradawi * 

Department of Chemistry and Earth Sciences, College of Arts and Sciences, Qatar University, Doha 2713, Qatar; kamelame@outlook.com (K.E.); yahiaashoeb@qu.edu.qa (Y.H.A.); asemata92@gmail.com (A.T.M.); anas.moustafa@qu.edu.qa (A.G.E.)

* Correspondence: siham@qu.edu.qa; Tel.: +974-4403-4666

Received: 17 August 2018; Accepted: 17 September 2018; Published: 22 September 2018



Abstract: Developing efficient catalyst for CO oxidation at low-temperature is crucial in various industrial and environmental remediation applications. Herein, we present a versatile approach for controlled synthesis of carbon nitride nanowires (CN NWs) doped with palladium and copper (Pd/Cu/CN NWs) for CO oxidation reactions. This is based on the polymerization of melamine by nitric acid in the presence of metal-precursors followed by annealing under nitrogen. This intriguingly drove the formation of well-defined, one-dimensional nanowires architecture with a high surface area ($120 \text{ m}^2 \text{ g}^{-1}$) and doped atomically with Pd and Cu. The newly-designed Pd/Cu/CN NWs fully converted CO to CO_2 at $149 \text{ }^\circ\text{C}$, that was substantially more active than that of Pd/CN NWs ($283 \text{ }^\circ\text{C}$) and Cu/CN NWs ($329 \text{ }^\circ\text{C}$). Moreover, Pd/Cu/CN NWs fully reserved their initial CO oxidation activity after 20 h. This is mainly attributed to the combination between the unique catalytic properties of Pd/Cu and outstanding physicochemical properties of CN NWs, which tune the adsorption energies of CO reactant and reaction product during the CO oxidation reaction. The as-developed method may open new frontiers on using CN NWs supported various noble metals for CO oxidation reaction.

Keywords: carbon nitride; nanowires; CO oxidation; noble metal catalysts

1. Introduction

Carbon nitride (CN) materials have attracted much great attention in the past few decades, owing to their outstanding physicochemical properties such as great thermal/chemical stability, electric conductivity, and mechanical properties [1–5]. These properties enabled the successful utilization of CN materials in various catalytic and industrial applications [1–5]. The CO preferential oxidation (CO-PROX) in an H_2 -rich stream is among the most important catalytic reactions in various industrial process and environmental applications [6–10]. Additionally, the CO-PROX is an effective approach for providing clean H_2 in polymer electrolyte membrane fuel cells along with decreasing the concentration of CO to be below 10–100 ppm [10–12]. Various catalysts including noble metals and metal-oxides supported on TiO_2 , SiO_2 , and Ce_2O_3 were developed for efficient CO oxidation [10–12]. Compared with these catalysts and/or supports, CN-based materials are more abundant, cost-effective, and can be easily synthesized with high yield. Furthermore, CN materials are highly stable chemically and thermally at high operating temperatures, which are required features in large-scale applications [10–13]. Moreover, the dissimilar electron density between C and N in CN materials can greatly enhance the interaction with metal-based catalysts and

accelerate the electron mobility during catalytic reactions [13]. Noticeably, the CO oxidation performance on CN-based materials was rarely reported relative to other catalytic applications [14,15]. Generally, the functionalization of CN-based materials with metal-based catalysts can greatly improve their catalytic activity [16–19]. For instance, CN/silica-supported Pt nanoparticles achieved a complete CO conversion at 160 °C, which was significantly more active than silica-supported Pt nanoparticles (250 °C) [20]. This indicates the significant effect of CN supporter on enhancement the CO oxidation activity of Pt. Recently, the theoretical studies revealed the lower energy barrier for CO oxidation on g-C₃N₄/Pt relative to on pure Pt that originated from the strong electronic interaction between Pt and C₃N₄ [21].

Unlike other metal-based catalysts, Cu-based and Pd-based catalysts are well known with their supreme CO oxidation activity and stability [22–27]. Both metals have an outstanding ability to provide active sites for activation and dissociation of O₂ during CO oxidation reaction [22–27]. Moreover, the great O₂-adsorption affinity of Cu and its ability to originate oxygenated species that can accelerate the CO oxidation kinetics at lower temperatures [28]. Meanwhile, Pd with its great CO-adsorption affinity provides high tolerance for adsorption of CO₂ product [29]. Various studies reported the CO oxidation activity of Pd-based and Cu-based catalyst supported on various supports such as ceria and other metal oxides [25,30,31]. However, using CN-based materials as supports for Pd-based and/or Cu-based catalyst for CO oxidation reaction was rarely reported. For example, Cu₂O/C₃N₄ exhibited 100% CO conversion at 200 °C, while Cu₂O only exhibited only 3% CO conversion at 220 °C [15]. This is originated from the strong electronic interaction between g-C₃N₄ and Cu₂O along with the well-dispersion of Cu₂O on g-C₃N₄ [15].

One-dimensional CN-based nanowires possess various advantages over other zero-dimensional nanostructures such as inbuilt high accessible surface area, low-density, and multiple active surface sites, and strong electronic interactions. However, fabrication of CN-based nanowires was not emphasized enough relative to other one-dimensional nanostructures such as rods, fiber, and needles [32–35]. Hence, the combination between unique physicochemical properties of CN NWs and outstanding catalytic properties of Pd and Cu can enhance the CO oxidation activity significantly.

Herein, we present a versatile approach for precise fabrication of Pd/Cu/CN NWs via the polymerization of melamine by nitric acid in the presence of metal precursors followed by carbonization. This drove the formation of one-dimensional nanowires with a great surface area and doped atomically with Pd and Cu. The CO oxidation performance of Pd/Cu/CN NWs was benchmarked relative to Pd/CN NWs, Cu/CN NWs, and CN NWs. The presented method may open new borders on using CN NWs supported metal-based catalysts for CO oxidation.

2. Results and Discussion

Pd/Cu/CN NWs were typically prepared by the polymerization of melamine by nitric acid in the presence of metal precursors followed by consecutive pyrolysis under nitrogen. Figure 1a shows the SEM image of Pd/Cu/CN NWs formed in high yield (nearly 100%) of nanowire morphology. The average length of nanowires is 2 μm and a width of 80 nm (Figure 1b). The TEM (transmission electron microscope) image also confirmed the formation of a one-dimensional nanowire structure (Figure 1c). The nanowires were highly uniform and mono-dispersed without any undesired spherical nanoparticles (Figure 1d). The high magnification TEM of randomly selected nanowire also displayed the production of one-dimensional nanowire structure with a smoothed surface (Figure 2a). The high-resolution TEM (HRTEM) revealed the amorphous-crystalline phase of CN NWs agrees with elsewhere reports (Figure 2b,c) [36–38]. The absence of Pd and Cu metals in the HRTEM images suggests their atomic doping inside the CN NWs structures without the formation of bimetallic PdCu alloy. This is due to the absence of any reducing agent in the synthetic procedure. Interestingly, the Fourier filtered images showed that the lattice fringes in the shell area were twisted and well-oriented across the wire-wall as shown as an insight in Figure 2b. Meanwhile, the lattice fringes in the core area were randomly aligned and contain various defects, shown as an insight in

Figure 2c. These defects are originated from the atomic distribution of Pd and Cu inside the CN NWs lattice structure. The determined d-spacing in both core and shell areas was about (0.34 nm) that was assigned to {002} facets of graphitic-like carbon structure. This agrees with the selected-area electron diffraction (SAED) pattern (Figure 2d).

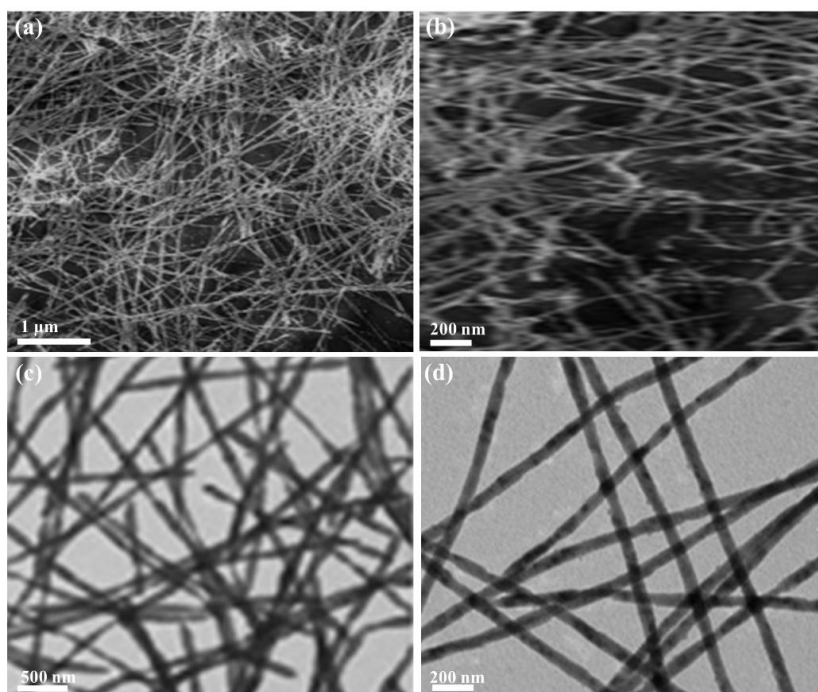


Figure 1. (a,b) SEM images and (c,d) TEM images of Pd/Cu/CN NWs prepared under typical conditions.

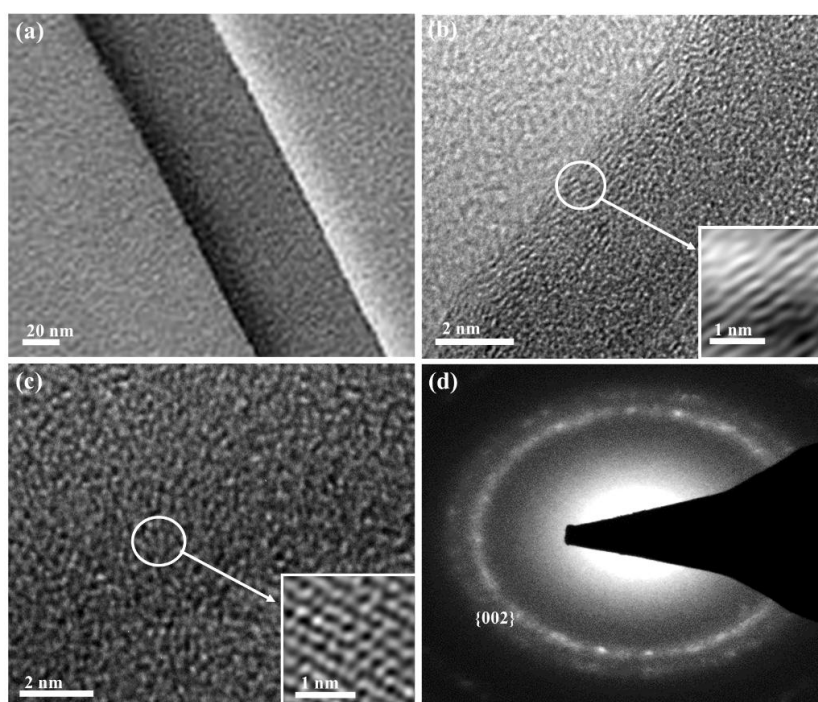


Figure 2. (a) High magnification TEM image of Pd/Cu/gCN NWs; (b,c) HRTEM images; and (d) SAED pattern of Pd/Cu/CN NWs. The insights show the corresponding Fourier filtered images for the marked areas in (b,c), respectively.

As a reference, metal free, one-dimensional CN NWs were prepared by the same synthetic method of Pd/Cu/CN NWs but without metal precursors (Figure S1). The average length of CN NWs was nearly 2.1 μm and 75 nm in width. Interestingly, the average width of the as-synthesized CN NWs was slightly smaller than that of Pd/Cu/CN NWs, attributed to the integration of Pd and Cu into CN lattice structure.

The high-angle annular dark-field scanning TEM (HAADF-STEM) also confirmed the formation of one-dimensional nanowire structure with a smoothed surface (Figure 3a). The element mapping analysis of Pd/Cu/CN NWs clearly demonstrated the homogenous distribution of C, N, Cu, and Pd with atomic ratios of 41, 57.8, 0.5, and 0.7, respectively (Figure 3b–e). The composition of Pd/Cu/CN NWs was further investigated by the EDX (energy dispersive spectrometer) analysis that displayed the presence of C, N, Pd, and Cu. Meanwhile, CN NWs showed only the presence of C and N with an atomic ratio 41/59 (Figure 3f). The estimated composition of the as-synthesized materials was almost in line with the initial precursor's concentrations.

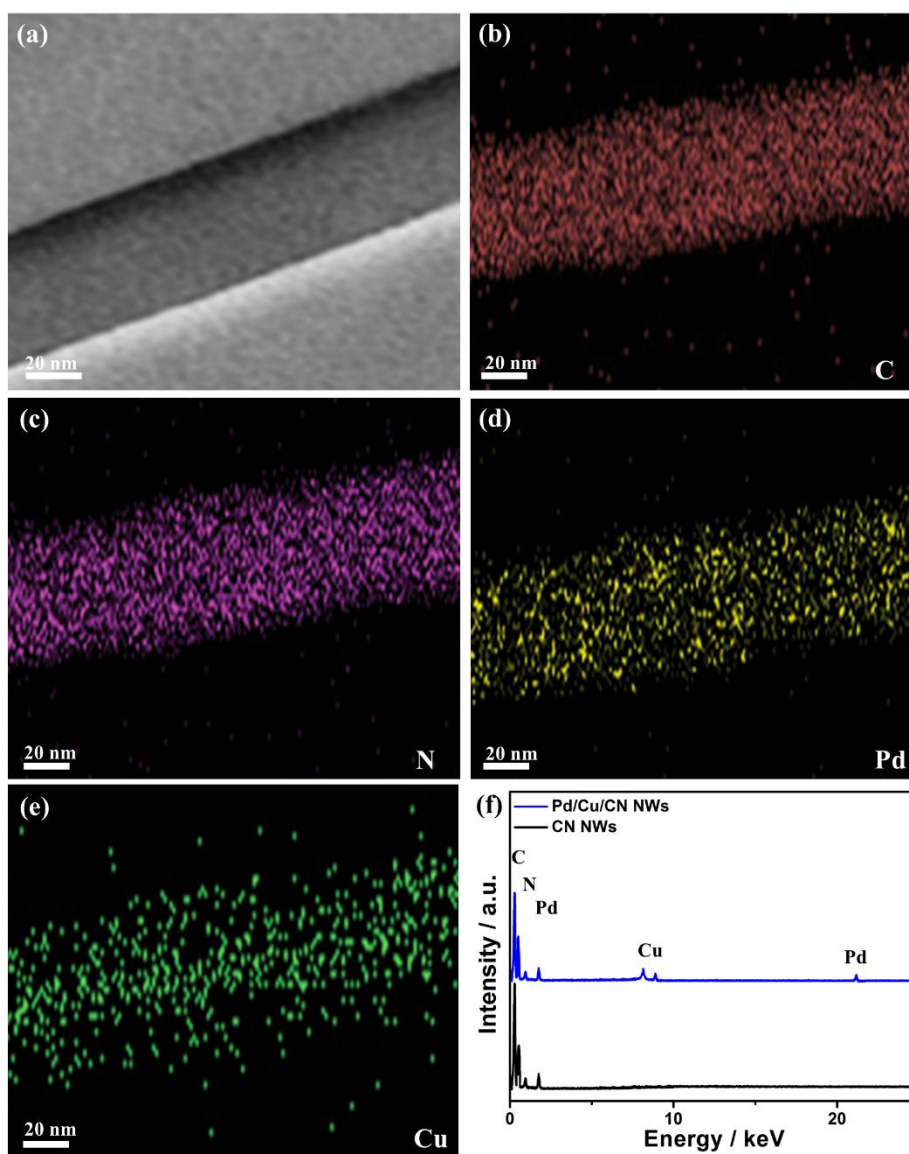


Figure 3. (a) HAADF-STEM image of an individual Pd/Cu/CN NWs and its elemental mapping analysis for (b) C; (c) N; (d) Pd; and (e) Cu; (f) the EDX analysis of both Pd/Cu/CN NWs and CN NWs.

Figure 4a shows the XRD (X-ray diffraction pattern) patterns of the Pd/Cu/CN NWs and CN NWs, which both depicted the presence of a single broad peak at 27.6° attributes to the {002} facet of graphitic-like carbon (Figure 4a). Interestingly, the diffraction pattern of Pd/Cu/CN NWs was shifted towards a higher 2θ value relative to pure CN NWs, which indicates the presence of Pd and Cu inside the CN-skeleton structure. Notably, we couldn't resolve any XRD diffraction peaks for Pd or Cu and/or their oxides, indicates their atomic doping inside the CN matrix. This is also may be due to the low concentration of Pd/Cu.

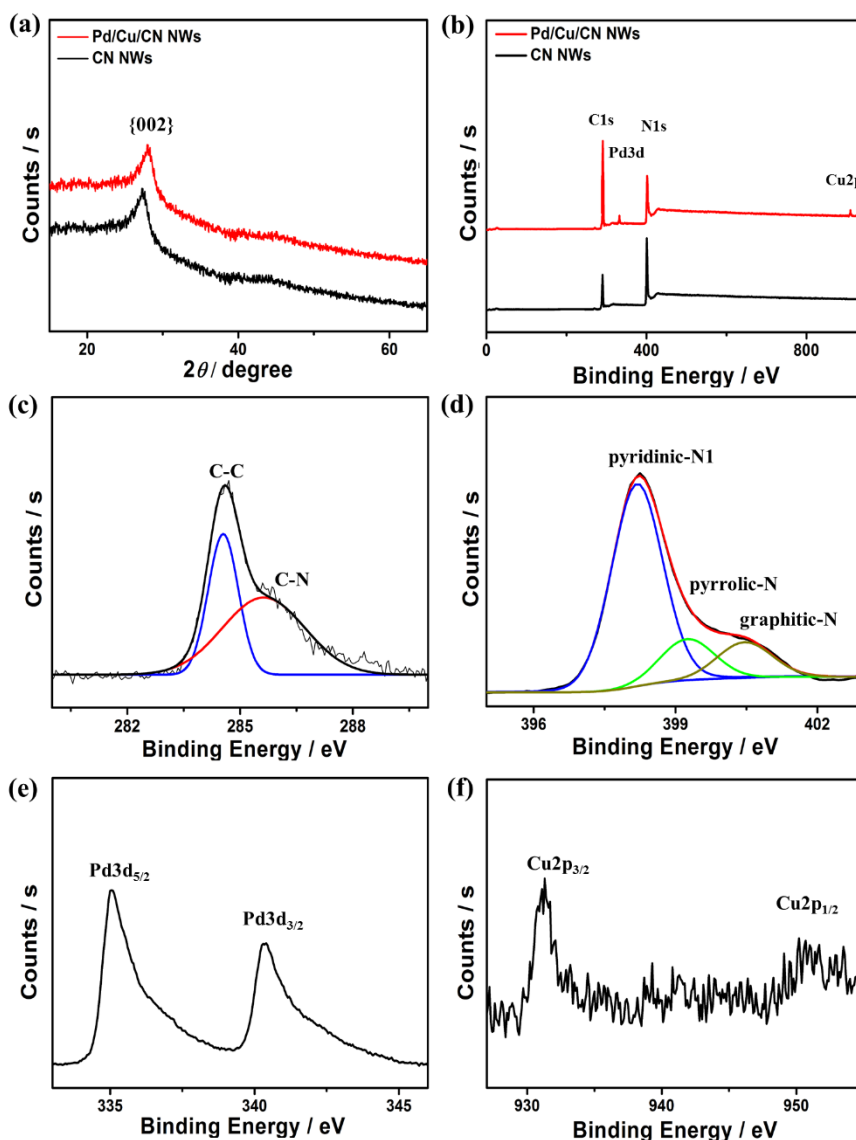


Figure 4. (a) Wide-angle XRD patterns; (b) XPS survey of Pd/Cu/CN NWs and CN NWs; (c) high resolution XPS spectra of C; (d) N; (e) Pd; and (f) Cu.

The surface chemical state and composition of the as-obtained materials were estimated by the XPS (X-ray photoelectron spectroscopy) analysis. The XPS survey of Pd/Cu/CN NWs depicted the existence of C, N, Pd, and Cu peaks, whereas CN NWs displayed only C and N peaks (Figure 4b). The C and N peaks of Pd/Cu/CN NWs were positively shifted to higher binding energies relative to their counterparts of CN NWs, ascribed to the Pd and Cu dopants. The high-resolution XPS spectra of C1s were fitted into two mean peaks at 284.6 and 286.7 eV, assigned to C-C and C-N, respectively (Figure 4c). The N 1s spectra were deconvoluted into three peaks at 398.6, 400.0, and 401.7 eV corresponded to pyridinic-N, pyrrolic-N, and graphitic-N, respectively (Figure 4d), demonstrates the

formation of carbon nitride structure. The resolved Pd 3d spectra were attributed to Pd 3d_{5/2} at 335.0 eV and Pd 3d_{3/2} at 340.5 eV (Figure 4f). Meanwhile, the resolved Cu 2p peaks were assigned to Cu 2p_{3/2} at 932.1 eV and Cu 2p_{1/2} at 951.2 eV (Figure 4f). This implies that both Pd and Cu are in the metallic state without any significant oxide phases that might be attributed to their atomic doping. Interestingly, the Pd 3d and Cu 2p peaks were not shifted relative to their pure metallic phases, suggests the absence of any electron transfer between them. This attributes to the absence of any kind of bimetallic PdCu alloy. The surface composition of the as-synthesized materials estimated by the XPS showed that the atomic ratio of C/N/Pd/Cu were about 40/59/0.4/0.6, correspondingly. These ratios are different from the real composition, due to the fact that XPS measures only the surface composition. The XPS results clearly displayed the absence of any undesired by-products such as oxygen, K⁺, and NO₃⁻, which indicates the purity of the as-formed materials agrees with the EDX and element mapping analysis.

The formation of CN NWs was further confirmed by the Fourier transform infrared spectroscopy (FTIR) analysis (Figure S2). The FTIR spectrum revealed a strong absorption band at 810 cm⁻¹ assigned to the breathing mode of triazine [39,40]. Additionally, the resolved obvious broad bands between 1200 and 1650 cm⁻¹ were attributed to the stretching mode of C-N [39]. Meanwhile, the small band at 3500 cm⁻¹ is assigned to the N-H [41]. The slight shifting in the FTIR peaks of Pd/Cu/CN NWs relative to CN NWs plausibly originated from the Pd and Cu dopants.

The BET surface area of Pd/Cu CN NWs was determined to be (120 m² g⁻¹), which was slightly higher than that of CN NWs (110 m² g⁻¹) (Figure 5). The slightly higher surface area of Pd/Cu/CN NWs may be attributed to the defects inside the CN lattice structure made by Pd and Cu dopants. Fabrication of Pd/Cu/CN NWs with a high surface area was favored for providing various accessible active sites during the CO oxidation reaction.

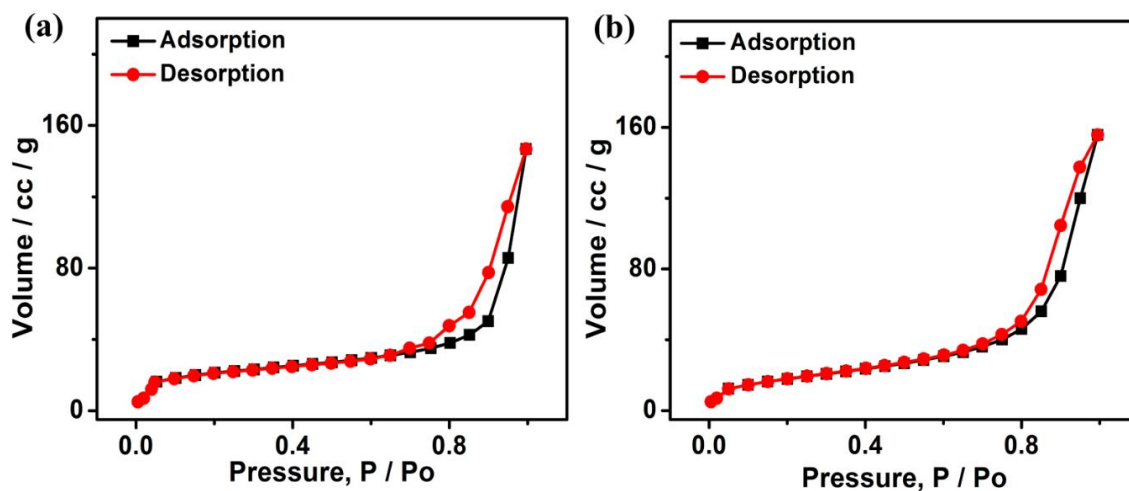
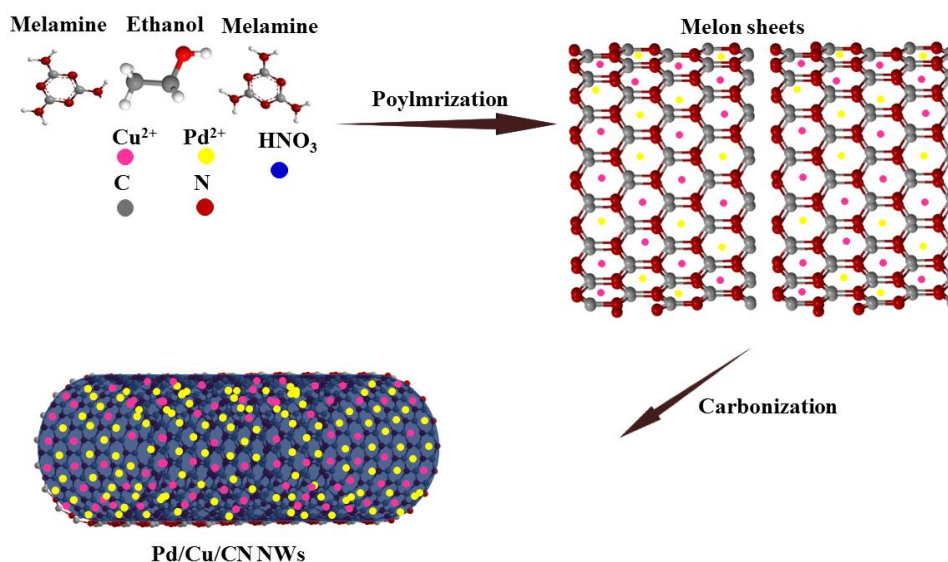


Figure 5. (a) N₂ adsorption-desorption isotherms of Pd/Cu/CN NWs and (b) CN NWs.

The formation process of Pd/Cu/CN NWs was optimized and adjusted via various reaction experiments. The sluggish addition of melamine into ethanol is critical to avoid the formation of aggregated nanosheets (Figure S3a). This is because of that, the slow addition of melamine led to a strong Van der Waals forces, which bind melamine sheets together during polymerization step and facilitate their wrapping into a nanowires structure. Likewise, the quick addition of nitric acid formed aggregated nanosheets (Figure S3b), while reducing the concentration of nitric acid to (0.05 M) produced non-uniform nanowires (Figure S3c). Increasing the concentration of nitric acid to 0.15 M formed nanowires morphology with a larger width (95 nm) (Figure S3d). These results indicated the significant role of nitric acid to direct the formation of uniform nanowires structure.

Talking into our considerations these results the fabrication process of Pd/Cu/CN NWs can be attributed to the polymerization of melamine followed by carbonization at elevated temperatures

(Scheme 1). Particularly, nitric acid activates melamine to heptazine, which subsequently polymerized to form a sheet-like structure of melon via the removing of NH_3 . Meanwhile, Pd and Cu adsorbed simultaneously on the N-atoms of melon. These melon sheets were bonded together by strong Van der Waals forces and then conversion into nanowires structures. Finally, the melon nanowires converted to carbon nitride after pyrolysis at high temperatures under nitrogen.



Scheme 1. The hypothesized formation mechanism of Pd/Cu/CN NWs.

Various carbon nitride-based materials with and without metal-based catalyst were prepared by different methods for various catalytic applications [42–46]; however, their CO oxidation performance was rarely reported. Additionally, the controlled synthesis of one-dimensional CN nanowires doped with multiple metal-based catalysts wasn't emphasized enough relative to other structures. Thus, the combination between unique physicochemical properties of CN NWs with outstanding catalytic properties of Pd and Cu can greatly enhance their catalytic activity towards various reactions.

Inspired by the impressive structure and composition features of Pd/Cu/CN NWs, their CO oxidation performance was benchmarked under atmospheric condition relative to Pd/CN NWs, Cu/CN NWs, and CN NWs. The percentage of the CO conversions (CO %) on the as-made catalysts was measured as a function of the temperature (Figure 6). The results showed that metal-free CN NWs only converted 8% of CO at 420 °C (Figure 6). Meanwhile, after doping, CN-NWs with Pd and/or Cu the CO conversion % increased substantially by increasing the reaction temperatures (Figure 6). To this end, Pd/CN NWs and Cu/CN-NWs achieved a full CO conversion at 283 °C and 329 °C, respectively. This shows the significant role of Pd and Cu on enhancement the CO conversion efficiency of CN NWs. Interestingly, Pd/Cu/CN NWs converted CO completely to CO_2 at 149 °C. This implies the substantial electronic effect of Pd/Cu and their synergetic effect with CN NWs on boosting the CO oxidation kinetics at a lower temperature. This is further observed in the quick CO oxidation kinetics on Pd/Cu/CN NWs than that on Pd/CN NWs and Cu/CN NWs at any temperature as indicated by the dashed lines in Figure S4a. Thus, the complete conversion temperature (T_{100}) of Pd/Cu/CN NWs (149 °C) was significantly lower than that of Pd/CN NWs by 134 °C and Cu/CN NWs by 180 °C (Figure S4b). This is due to the strong CO-adsorption and O_2 -adsorption ability of Pd and Cu, respectively, which accelerate the CO oxidation reaction kinetics. Interestingly, compared with other Pd-based and Cu-based catalyst reported previously, our newly synthesized Pd/Cu/CN NWs displayed a superior CO oxidation activity (Table S1) [47,48]. The catalytic activities of different synthesized catalysts were evaluated at 120 °C by calculating the rate of CO oxidation. The calculated CO oxidation rates for the catalysts are 0.88, 0.076, and 0.024 $\mu\text{mol s}^{-1} \text{g}_{\text{cat}}^{-1}$ for Pd/Cu/CN NWs,

Pd/CN NWs, and Cu/CN NWs, respectively. It should be noticed that, the amount of CO₂ produced matches with the CO consumed (Figure S5).

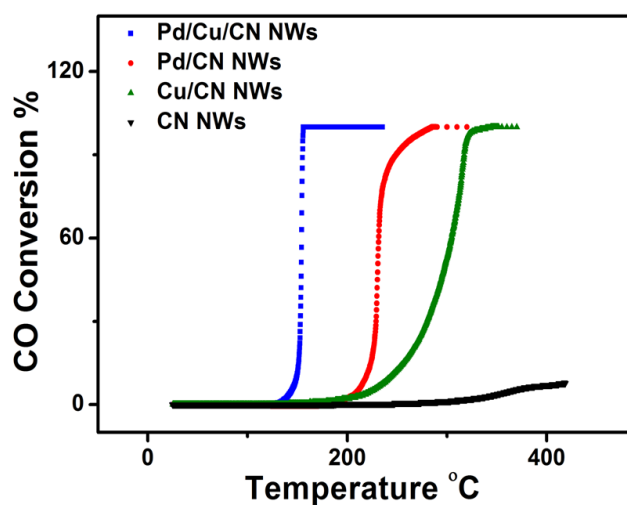


Figure 6. CO conversion efficiency on the as-synthesized Pd/Cu/CN NWs, Pd/CN NWs, Cu/CN NWs, and CN NWs as a function of temperature.

The durability tests of Pd/Cu/CN NWs were carried out for 20 h relative to Pd/CN NWs and Cu/CN NWs at their half conversion temperature (T_{50}) (Figure 7). Intriguingly, Pd/Cu/CN NWs reserved their initial CO oxidation activity without any significant loss after 20 h; meanwhile, Pd/CN NWs and Cu/CN NWs displayed a slight decrease in their initial activity (Figure 7). This is owing to coupling between the electronic effect of Pd/Cu and CN NWs that tune the adsorption of reactant and reaction products. Intriguingly, Pd/Cu/CN NWs kept their nanowire morphology after the durability tests (Figure S6).

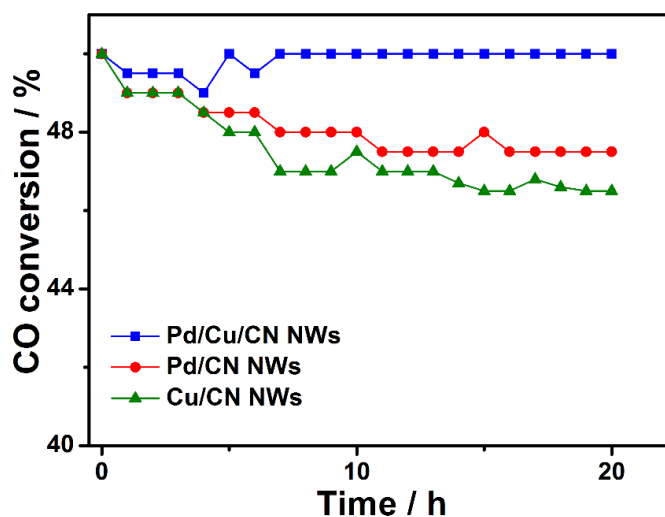


Figure 7. The stability tests the as-prepared catalysts measured for 20 h at T_{50} .

Talking into our consideration these results, the superior CO oxidation activity and durability of Pd/Cu/CN NWs originated from the structure and composition effects [19–28]. Indeed, one-dimensional nanowires morphology with outstanding surface area provided more accessible active sites for the adsorption of O₂ and CO molecules. Meanwhile, the strong O₂ adsorption affinity of Cu and CO-adsorption affinity of Pd tune the adsorption of reactants and reaction products [19–28]. Additionally, Cu can originate various oxygenated species, which accelerate the CO oxidation kinetics

at low temperature [19–28]. The atomic distribution of Pd and Cu inside the CN skeleton structure is not vulnerable to aggregation and/or losing the active sites. Thus, the combination between CN NWs and Pd/Cu balances between strong CO oxidation activity and durability.

3. Experimental

3.1. Chemicals and Materials

$K_2PdCl_4 \cdot 6H_2O$ (99.99%), $CuCl_2 \cdot 6H_2O$ (99%), melamine (99%), ethanol (99%), and nitric acid (HNO_3 (98%)) were obtained from Sigma-Aldrich Chemie GmbH (Munich, Germany).

3.2. Synthesis of Pd/Cu/gCN NWs

In the typical synthesis of Pd/Cu/CN NWs, 1 g of melamine was dissolved in 30 mL of ethanol solution containing 20 mM of K_2PdCl_4 and 20 mM of $CuCl_2$ under stirring for 30 min. Then, 60 mL of HNO_3 (0.2 M) was slowly added to the previous mixture and kept under stirring until the formation of white precipitation. This precipitate was subsequently washed with ethanol and dried in a vacuum at 80 °C for 12 h. This was followed by pyrolysis at 400 °C (3 °C min^{-1}) under N_2 in tube-furnace for 2 h. The final Pd/Cu/CN NWs products were obtained after cooling to room temperature and were kept for further characterization.

3.3. Materials Characterization

The morphological characterization of the as-obtained materials was conducted on a scanning electron microscopy (SEM, Hitachi S-4800, Hitachi, Tokyo, Japan) a transmission electron microscope (TEM, TecnaiG220, FEI, Hillsboro, OR, USA) equipped with energy dispersive spectrometer (EDS). The X-ray photoelectron spectroscopy (XPS) was analyzed on a Kratos Axis (Ultra DLD XPS Kratos, Manchester, UK) spectrometer equipped with a monochromatic Al $K\alpha$ radiation source (1486.6 eV) under a UHV environment (ca. 5×10^{-9} Torr). The X-ray diffraction pattern (XRD) was measured on an X-ray diffractometer (X'Pert-Pro MPD, PANalytical Co., Almelo, Netherlands) using Cu $K\alpha$ X-ray source ($\lambda = 1.540598\text{ \AA}$). The N_2 -physisorption isotherms were measured on a Quantachrome Instrument Corporation Autosorb-1 analyzer (Quantachrome Instrument Corporation, Boynton Beach, FL, USA), whereas, the surface area was estimated using a Brunauer-Emmett-Teller (BET) calculated from the adsorption data in the relative pressure. The Fourier transform infrared spectra were recorded on a Thermo Nicolet Nexus 670 FTIR spectrometer (Thermo Scientific, Madison, WI, USA).

3.4. CO Oxidation Reaction

The catalytic activity of the obtained materials was investigated towards the CO oxidation reaction. Particularly, 50 mg of each catalyst was pretreated at 250 °C under air (50 mL min^{-1}) for 1 h in a fixed bed quartz tubular reactor with an inner diameter of 6 mm followed by purging 50 mL min^{-1} of H_2 stream for 1 h prior to the CO oxidation measurements. Then, after cooling the catalysts were exposed to the gas mixture involves 4% CO, 20% O_2 , and the balance is Ar, with a total flow of 50 mL min^{-1} . The CO conversion efficiency to CO_2 was estimated using an online gas analyzer (IR200, Yokogawa, Japan) at different temperatures ranging between 25 and 450 °C. The percentage of CO conversion efficiency (CO %) was calculated using the following equation:

$$CO\ (\%) = [(CO_{in} - CO_{out})]/CO_{in} \times 100$$

where CO_{in} is the input concentration and CO_{out} is the output concentration.

4. Conclusions

In summary, a facile method is presented for controlled synthesis of Pd/Cu/CN NWs as an efficient catalyst for CO oxidation reaction. This includes the activation of melamine in ethanol

solution by nitric acid in the presence of metal salts followed by carbonization at a high temperature. This drove the formation of well-defined one-dimensional nanowires architecture with a high aspect ratio, great surface area, and well-dispersed Pd and Cu. The as-formed NWs displayed a superior catalytic activity and durability towards CO oxidation reaction. Indeed, Pd/Cu/CN NWs achieved a full CO conversion at 149 °C that was significantly higher than that of Pd/CN NWs (283 °C) and Cu/CN NWs (329 °C). This originated from the combination between catalytic properties of Pd/Cu and physicochemical properties of CN NWs, which tune the adsorption and activation of reactants (O₂ and CO) and reaction product (CO₂). The presented approach may be applicable for the controlled synthesis of various CN NWs loaded with multiple metal-based catalysts for different applications.

Supplementary Materials: The following are available online at <http://www.mdpi.com/2073-4344/8/10/411/s1>, Figure S1: (a) SEM image and (b) TEM image of metal free CN NWs, Figure S2: FTIR spectrum of Pd/Cu/CN NWs and CN NWs, Figure S3: TEM images of Pd/Cu CN NWs obtained by (a) quick addition of melamine, (b) quick addition of HNO₃, (c) using 60 mL of HNO₃ (0.05 M), (d) using 60 mL of HNO₃ (0.15 M), Figure S4: (a) the CO conversion efficiency on the as-synthesized catalysts at temperature ranging between 25 and 200 °C, (b) the complete conversion temperature T100, Figure S5: The CO₂ produced relative to CO consumed during the CO oxidation reaction, Figure S6: TEM image of Pd/Cu CN NWs before (a) and after (b) stability tests, Table S1: Comparison between the CO oxidation activity of our newly designed Pd/Cu/CN NWs and various Pd-based and Cu-based catalyst reported previously.

Author Contributions: K.E. and Y.H.A. contributed equally to the work. A.T.M. and A.G.E. carried out the synthesis and CO oxidation measurement. S.Y.A.-Q. supervised the group.

Funding: This research was funded by Qatar National Research Fund 7-485-1-091.

Acknowledgments: This work was made possible by NPRP Grant no. NPRP 7-485-1-091 from the Qatar National Research Fund (a member of Qatar Foundation). The statements made herein are solely the responsibility of the authors. The publication of this article was funded by the Qatar National Library.

Conflicts of Interest: There are no conflicts to declare.

References

1. Wang, X.; Blechert, S.; Antonietti, M. Polymeric graphitic carbon nitride for heterogeneous photocatalysis. *Acs Catal.* **2012**, *2*, 1596–1606. [[CrossRef](#)]
2. Zhang, H.; Zuo, X.; Tang, H.; Li, G.; Zhou, Z. Origin of photoactivity in graphitic carbon nitride and strategies for enhancement of photocatalytic efficiency: Insights from first-principles computations. *Phys. Chem. Chem. Phys.* **2015**, *17*, 6280–6288. [[CrossRef](#)] [[PubMed](#)]
3. Zhang, K.; Wang, L.; Sheng, X.; Ma, M.; Jung, M.S.; Kim, W.; Lee, H.; Park, J.H. Tunable bandgap energy and promotion of H₂O₂ oxidation for overall water splitting from carbon nitride nanowire bundles. *Adv. Energy Mater.* **2016**, *6*, 1502352. [[CrossRef](#)]
4. Luan, P.; Zhang, Y.; Zhang, X.; Li, Z.; Prathapan, R.; Bach, U.; Zhang, J. Bismuth vanadate with electrostatically anchored 3d carbon nitride nano-networks as efficient photoanodes for water oxidation. *ChemSusChem* **2018**, *11*, 2510–2516. [[CrossRef](#)] [[PubMed](#)]
5. Cui, W.; Li, J.; Dong, F.; Sun, Y.; Jiang, G.; Cen, W.; Lee, S.C.; Wu, Z. Highly efficient performance and conversion pathway of photocatalytic NO oxidation on SrO-clusters@amorphous carbon nitride. *Environ. Sci. Technol.* **2017**, *51*, 10682–10690. [[CrossRef](#)] [[PubMed](#)]
6. Wang, C.; Liu, S.; Wang, D.; Chen, Q. Interface engineering of Ru–Co₃O₄ nanocomposites for enhancing CO oxidation. *J. Mater. Chem. A* **2018**, *6*, 11037–11043. [[CrossRef](#)]
7. Twigg, M.V. Catalytic control of emissions from cars. *Catal. Today* **2011**, *163*, 33–41. [[CrossRef](#)]
8. Heck, R.M.; Farrauto, R.J. Automobile exhaust catalysts. *Appl. Catal. A Gen.* **2001**, *221*, 443–457. [[CrossRef](#)]
9. Wang, C.; Li, B.; Lin, H.; Yuan, Y. Carbon nanotube-supported Pt-Co bimetallic catalysts for preferential oxidation of CO in a H₂-rich stream with CO₂ and H₂O vapor. *J. Power Sources* **2012**, *202*, 200–208. [[CrossRef](#)]
10. Liu, K.; Wang, A.; Zhang, T. Recent advances in preferential oxidation of CO reaction over platinum group metal catalysts. *ACS Catal.* **2012**, *2*, 1165–1178. [[CrossRef](#)]
11. Morfin, F.; Nassreddine, S.; Rousset, J.; Piccolo, L. Nanoalloying effect in the preferential oxidation of CO over Ir–Pd catalysts. *Acs Catal.* **2012**, *2*, 2161–2168. [[CrossRef](#)]

12. Park, E.D.; Lee, D.; Lee, H.C. Recent progress in selective CO removal in a H₂-rich stream. *Catal. Today* **2009**, *139*, 280–290. [[CrossRef](#)]
13. He, F.; Li, K.; Yin, C.; Wang, Y.; Tang, H.; Wu, Z. Single Pd atoms supported by graphitic carbon nitride, a potential oxygen reduction reaction catalyst from theoretical perspective. *Carbon* **2017**, *114*, 619–627. [[CrossRef](#)]
14. Yang, H.; Lv, K.; Zhu, J.; Li, Q.; Tang, D.; Ho, W.; Li, M.; Carabineiro, S.A. Effect of mesoporous g-C₃N₄ substrate on catalytic oxidation of CO over Co₃O₄. *Appl. Surf. Sci.* **2017**, *401*, 333–340. [[CrossRef](#)]
15. Shi, Y.; Hu, X.; Zhao, J.; Zhou, X.; Zhu, B.; Zhang, S.; Huang, W. Co oxidation over Cu₂O deposited on 2d continuous lamellar gC₃N₄. *New J. Chem.* **2015**, *39*, 6642–6648. [[CrossRef](#)]
16. Li, S.-L.; Yin, H.; Kan, X.; Gan, L.-Y.; Schwingschlögl, U.; Zhao, Y. Potential of transition metal atoms embedded in buckled monolayer gC₃N₄ as single-atom catalysts. *Phys. Chem. Chem. Phys.* **2017**, *19*, 30069–30077. [[CrossRef](#)] [[PubMed](#)]
17. Ma, D.; Wang, Q.; Yan, X.; Zhang, X.; He, C.; Zhou, D.; Tang, Y.; Lu, Z.; Yang, Z. 3d transition metal embedded C₂N monolayers as promising single-atom catalysts: A first-principles study. *Carbon* **2016**, *105*, 463–473. [[CrossRef](#)]
18. Binder, A.J.; Qiao, Z.-A.; Veith, G.M.; Dai, S. Deposition–precipitation and stabilization of a silica-supported Au catalyst by surface modification with carbon nitride. *Catal. Lett.* **2013**, *143*, 1339–1345. [[CrossRef](#)]
19. Leng, K.; Mai, W.; Zhang, X.; Liu, R.; Lin, X.; Huang, J.; Lou, H.; Xie, Y.; Fu, R.; Wu, D. Construction of functional nanonetwork-structured carbon nitride with Au nanoparticle yolks for highly efficient photocatalytic applications. *Chem. Commun.* **2018**, *54*, 7159–7162. [[CrossRef](#)] [[PubMed](#)]
20. Xiao, P.; Zhao, Y.; Wang, T.; Zhan, Y.; Wang, H.; Li, J.; Thomas, A.; Zhu, J. Polymeric carbon nitride/mesoporous silica composites as catalyst support for Au and Pt nanoparticles. *Chem. Eur. J.* **2014**, *20*, 2872–2878. [[CrossRef](#)] [[PubMed](#)]
21. Wang, S.; Feng, Y.; Yu, M.; Wan, Q.; Lin, S. Confined catalysis in the g-C₃N₄/Pt (111) interface: Feasible molecule intercalation, tunable molecule–metal interaction, and enhanced reaction activity of CO oxidation. *ACS Appl. Mater. Interfaces* **2017**, *9*, 33267–33273. [[CrossRef](#)] [[PubMed](#)]
22. Wu, G.; Guan, N.; Li, L. Low temperature CO oxidation on Cu–Cu₂O/TiO₂ catalyst prepared by photodeposition. *Catal. Sci. Technol.* **2011**, *1*, 601–608. [[CrossRef](#)]
23. Mock, S.A.; Zell, E.T.; Hossain, S.T.; Wang, R. Effect of reduction treatment on CO oxidation with CeO₂ nanorod-supported cuox catalysts. *ChemCatChem* **2018**, *10*, 311–319. [[CrossRef](#)]
24. Slavinskaya, E.; Gulyaev, R.; Zadesenets, A.; Stonkus, O.; Zaikovskii, V.; Shubin, Y.V.; Korenev, S.; Boronin, A. Low-temperature CO oxidation by Pd/CeO₂ catalysts synthesized using the coprecipitation method. *Appl. Catal. B Environ.* **2015**, *166*, 91–103. [[CrossRef](#)]
25. Zhou, Y.; Wang, Z.; Liu, C. Perspective on CO oxidation over Pd-based catalysts. *Catal. Sci. Technol.* **2015**, *5*, 69–81. [[CrossRef](#)]
26. Su, Y.; Yuan, S.; Ning, D.; Zhang, Q.; Han, W.; Wang, Y. The template-free synthesis of CuO@CeO₂ nanospheres: Facile strategy, structure optimization, and enhanced catalytic activity toward CO oxidation. *Eur. J. Inorg. Chem.* **2018**, *2018*, 2927–2934. [[CrossRef](#)]
27. Ding, J.; Li, L.; Li, H.; Chen, S.; Fang, S.; Feng, T.; Li, G. Optimum preferential oxidation performance of CeO₂–CuO_x–rGO composites through interfacial regulation. *ACS Appl. Mater. Interfaces* **2018**, *10*, 7935–7945. [[CrossRef](#)] [[PubMed](#)]
28. Zhu, C.; Ding, T.; Gao, W.; Ma, K.; Tian, Y.; Li, X. CuO/CeO₂ catalysts synthesized from Ce–UiO-66 metal-organic framework for preferential CO oxidation. *Int. J. Hydrogen Energy* **2017**, *42*, 17457–17465. [[CrossRef](#)]
29. Spezzati, G.; Su, Y.; Hofmann, J.P.; Benavidez, A.D.; DeLaRiva, A.T.; McCabe, J.; Datye, A.K.; Hensen, E.J. Atomically dispersed Pd–O species on CeO₂ (111) as highly active sites for low-temperature CO oxidation. *ACS Catal.* **2017**, *7*, 6887–6891. [[CrossRef](#)] [[PubMed](#)]
30. Jin, M.; Park, J.-N.; Shon, J.K.; Kim, J.H.; Li, Z.; Park, Y.-K.; Kim, J.M. Low temperature CO oxidation over Pd catalysts supported on highly ordered mesoporous metal oxides. *Catal. Today* **2012**, *185*, 183–190. [[CrossRef](#)]
31. Lykaki, M.; Pachatouridou, E.; Carabineiro, S.A.; Iliopoulou, E.; Andriopoulou, C.; Kallithrakas-Kontos, N.; Boghosian, S.; Konsolakis, M. Ceria nanoparticles shape effects on the structural defects and surface chemistry: Implications in CO oxidation by Cu/CeO₂ catalysts. *Appl. Catal. B Environ.* **2018**, *230*, 18–28. [[CrossRef](#)]

32. Zhao, Y.; Liu, Z.; Chu, W.; Song, L.; Zhang, Z.; Yu, D.; Tian, Y.; Xie, S.; Sun, L. Large-scale synthesis of nitrogen-rich carbon nitride microfibers by using graphitic carbon nitride as precursor. *Adv. Mater.* **2008**, *20*, 1777–1781. [[CrossRef](#)]
33. Li, H.-J.; Qian, D.-J.; Chen, M. Templateless infrared heating process for fabricating carbon nitride nanorods with efficient photocatalytic H₂ evolution. *ACS Appl. Mater. Interfaces* **2015**, *7*, 25162–25170. [[CrossRef](#)] [[PubMed](#)]
34. Barrio, J.; Lin, L.; Amo-Ochoa, P.; Tzadikov, J.; Peng, G.; Sun, J.; Zamora, F.; Wang, X.; Shalom, M. Unprecedented centimeter-long carbon nitride needles: Synthesis, characterization and applications. *Small* **2018**, *14*, 1800633. [[CrossRef](#)] [[PubMed](#)]
35. Liu, J.; Huang, J.; Zhou, H.; Antonietti, M. Uniform graphitic carbon nitride nanorod for efficient photocatalytic hydrogen evolution and sustained photoenzymatic catalysis. *ACS Appl. Mater. Interfaces* **2014**, *6*, 8434–8440. [[CrossRef](#)] [[PubMed](#)]
36. Wang, N.; Li, X. Facile synthesis of CoO nanorod/C₃N₄ heterostructure photocatalyst for an enhanced pure water splitting activity. *Inorg. Chem. Commun.* **2018**, *92*, 14–17. [[CrossRef](#)]
37. Han, C.; Gao, Y.; Liu, S.; Ge, L.; Xiao, N.; Dai, D.; Xu, B.; Chen, C. Facile synthesis of aupd/g-C₃N₄ nanocomposite: An effective strategy to enhance photocatalytic hydrogen evolution activity. *Int. J. Hydrogen Energy* **2017**, *42*, 22765–22775. [[CrossRef](#)]
38. Le, S.; Jiang, T.; Li, Y.; Zhao, Q.; Li, Y.; Fang, W.; Gong, M. Highly efficient visible-light-driven mesoporous graphitic carbon nitride/ZnO nanocomposite photocatalysts. *Appl. Catal. B Environ.* **2017**, *200*, 601–610. [[CrossRef](#)]
39. Lotsch, B.V.; Schnick, W. From triazines to heptazines: Novel nonmetal tricyanomelaminates as precursors for graphitic carbon nitride materials. *Chem. Mater.* **2006**, *18*, 1891–1900. [[CrossRef](#)]
40. Wang, Y.; Hong, J.; Zhang, W.; Xu, R. Carbon nitride nanosheets for photocatalytic hydrogen evolution: Remarkably enhanced activity by dye sensitization. *Catal. Sci. Technol.* **2013**, *3*, 1703–1711. [[CrossRef](#)]
41. Hong, J.; Xia, X.; Wang, Y.; Xu, R. Mesoporous carbon nitride with in situ sulfur doping for enhanced photocatalytic hydrogen evolution from water under visible light. *J. Mater. Chem.* **2012**, *22*, 15006–15012. [[CrossRef](#)]
42. Wang, N.; Wang, J.; Hu, J.; Lu, X.; Sun, J.; Shi, F.; Liu, Z.-H.; Lei, Z.; Jiang, R. Design of palladium-doped g-C₃N₄ for enhanced photocatalytic activity towards hydrogen evolution reaction. *ACS Appl. Energy Mater.* **2018**, *1*, 2866–2873. [[CrossRef](#)]
43. Qu, D.; Liu, J.; Miao, X.; Han, M.; Zhang, H.; Cui, Z.; Sun, S.; Kang, Z.; Fan, H.; Sun, Z. Peering into water splitting mechanism of g-C₃N₄-carbon dots metal-free photocatalyst. *Appl. Catal. B Environ.* **2018**, *227*, 418–424. [[CrossRef](#)]
44. Song, X.; Yang, Q.; Yin, M.; Tang, D.; Zhou, L. Highly efficient pollutant removal of graphitic carbon nitride by the synergistic effect of adsorption and photocatalytic degradation. *RSC Adv.* **2018**, *8*, 7260–7268. [[CrossRef](#)]
45. Sui, X.-L.; Li, C.-Z.; Zhao, L.; Wang, Z.-B.; Gu, D.-M.; Huang, G.-S. Mesoporous g-C₃N₄ derived nano-titanium nitride modified carbon black as ultra-fine PtRu catalyst support for methanol electro-oxidation. *Int. J. Hydrogen Energy* **2018**, *43*, 5153–5162. [[CrossRef](#)]
46. Lu, N.; Bao, X.; Jiang, N.; Shang, K.; Li, J.; Wu, Y. Non-thermal plasma-assisted catalytic dry reforming of methane and carbon dioxide over g-C₃N₄-based catalyst. *Top. Catal.* **2017**, *60*, 855–868. [[CrossRef](#)]
47. Peterson, E.J.; DeLaRiva, A.T.; Lin, S.; Johnson, R.S.; Guo, H.; Miller, J.T.; Kwak, J.H.; Peden, C.H.; Kiefer, B.; Allard, L.F. Low-temperature carbon monoxide oxidation catalysed by regenerable atomically dispersed palladium on alumina. *Nat. Commun.* **2014**, *5*, 4885. [[CrossRef](#)] [[PubMed](#)]
48. Kumar, R.; Oh, J.-H.; Kim, H.-J.; Jung, J.-H.; Jung, C.-H.; Hong, W.G.; Kim, H.-J.; Park, J.-Y.; Oh, I.-K. Nanohole-structured and palladium-embedded 3d porous graphene for ultrahigh hydrogen storage and co oxidation multifunctionalities. *ACS Nano* **2015**, *9*, 7343–7351. [[CrossRef](#)] [[PubMed](#)]

